Research Article Vol. 30, No. 12 / 6 Jun 2022 / Optics Express 20952
Optics EXPRESS

Bio-inspired spherical compound eye camera for simultaneous wide-band and large field of view imaging

SHUANGSHUANG ZHANG,[1,2] QI WU,[1,2] CHENYANG LIU,[3] TAISHENG WANG,[1] HONGXIN ZHANG,[1] JINCHENG WANG,[1,2] YUE DING,[1,2] JINPENG CHI,[1,2] WENBIN XU,[1] YANG XIANG,[1] AND CHENGYONG SHI[1,*]

[1]*R&D Center of Precision Instruments and Equipment, Changchun Institute of Optics, Fine Mechanics & Physics, Chinese Academy of Sciences, No.3888, Dongnanhu Road, Changchun, Jilin 130033, China*
[2]*University of Chinese Academy of Sciences, Beijing 100049, China*
[3]*School of Science, Hainan University, No.58, Renmin Road, Haikou, Hainan 570228, China*
[*]*shichengyong@ciomp.ac.cn*

Abstract: Natural compound eyes have excellent optical characteristics, namely large field of view, small size, no aberration, and sensitive to motion. Some arthropods have more powerful vision. For example, the Morpho butterfly's compound eyes can perceive the near-infrared and ultraviolet light that the human eye cannot see. This wide-band imaging with a large field of view has great potential in wide-area surveillance, all-weather panoramic imaging, and medical imaging. Hence, a wide-band spherical compound eye camera inspired by the Morpho butterfly's eye was proposed. The wide-band spherical compound eye camera which can achieve a large field of view ($360° \times 171°$) imaging over a wide range of wavelengths from 400nm to 1000nm, mainly consists of three parts: a wide-band spherical compound eye with 234 sub-eyes for light collection, a wide-band optical relay system for light transmission, and a wide-band CMOS image sensor for photoelectric conversion. Our experimental results show that the wide-band spherical compound eye camera not only captures a large field of view without anomalous blurring or aberrations but also perceives near-infrared light that is not recognized by the human eye. These features make it possible for distortion-free panoramic vision and panoramic medical diagnosis.

1. Introduction

The visual information captured by the eyes is crucial to many animals for finding food, suitable habitats, and conspecifics, as well as identifying and locating predators. Due to the unique living habits of different species of animals, the size and shape of their eyes have changed over time [1]. There are mainly two types of eyes in nature: monocular eyes like human eyes and compound eyes found in arthropods. Traditional monocular large field of view imaging systems such as fisheye lenses have severe distortion. For example, a Canon fisheye lens (EF 8-15 mm f/4L USM) with a field of view of 180° has a distortion of up to 50%. Different from human eyes, compound eyes are characterized by a variable number of small eyes, ommatidia, which are oriented to receive light from different directions. This makes compound eyes have the advantages of small size, large field of view, no aberration, and even high sensitivity to motion [2–5].

The current research on the bionic compound eye camera mainly focuses on three aspects: Planar compound eye camera for obtaining three-dimensional (3D) information [6] or reducing the size of the camera [7,8]; Planar compound eye camera for color [9] and near-infrared imaging [10]; Curved compound eye camera for capturing panoramic image [11,12] or multispectral imaging [13,14]. The range of wavelengths of the planar compound eye camera has been extended to near-infrared, not limited to the visible light. Although some planar compound eye cameras

#454530 https://doi.org/10.1364/OE.454530
Journal © 2022 Received 25 Jan 2022; revised 6 Apr 2022; accepted 11 May 2022; published 26 May 2022

Optics EXPRESS

with a large field of view have been proposed, such as catadioptric planar compound eye which has a field of view of 90.7° [15]. However, its inherent structural characteristics make it difficult to achieve larger field of view imaging. Most curved compound eye cameras, which easily acquire large field of view images, work in the range of visible light and have low resolution. For example, RSCEs and digital camera have fields of view up to 160°and 165° respectively [11,16]. But both of them have very low pixel resolution and cannot achieve high resolution imaging. In summary, most of the proposed compound eye cameras have low resolution, narrow working range, and insufficient field of view, which greatly limit its application. It is necessary to seek a wide band and large field of view imaging solution without abnormal blurring and distortion.

In nature, the compound eyes of some arthropods can also perceive the invisible light humans cannot access with the naked eye. The bee's eye can recognize most colors as human eye does, and have adapted well to see blue, green, and ultra-violet (UV) light. This allows them to see colors and ultraviolet nectar guides on flowers which guide bees to the nectar [17,18]. The Morpho butterfly, whose eyes are sensitive to the UV, visible, and near-infrared (NIR) spectra, has better vision [19]. The best visual system in the animal kingdom is the Mantis shrimp's eye, which can perceive the world through 16 channels of color and detect UV, NIR, and even polarized light [20–23]. These unique compound eyes can achieve panoramic imaging and be sensitive to a wider range of light to enhance vision. Simultaneous wide-band and large field of view imaging has great application potential in the fields of medical diagnosis, target recognition, surveillance, and reconnaissance.

To realize simultaneous wide-band and large field of view imaging, we developed a wide-band spherical compound eye camera which can achieve a large field of view ($360° \times 171°$) imaging over a range of wavelengths from 400nm to 1000nm. The wide-band spherical compound eye camera, inspired by the Morpho butterfly's apposition compound eyes (see Fig. 1(a) and (b)), consists of three parts: a wide-band spherical compound eye with 234 sub-eyes for light collection, a wide-band optical relay system for light transmission, and a wide-band CMOS image sensor for photoelectric conversion. The picture and schematic diagram of this camera are shown in Fig. 1(c) and (d) respectively. Among them, the spherical compound eye is composed of 234 independent and non-interfering visual units arranged on a 3D printed resin spherical shell. The primary images formed by those visual units are re-imaged on a CMOS sensor by an optical relay system similar to the crystalline cone. Thanks to the powerful adjustment capabilities of the optical relay system, this spherical compound eye camera can capture clear images over a wide range of wavelengths, from visible to NIR. This wide-band compound eye camera with a large field of view can be widely used in the fields of target detection, recognition, surveillance, reconnaissance, and medical diagnosis.

Optics EXPRESS

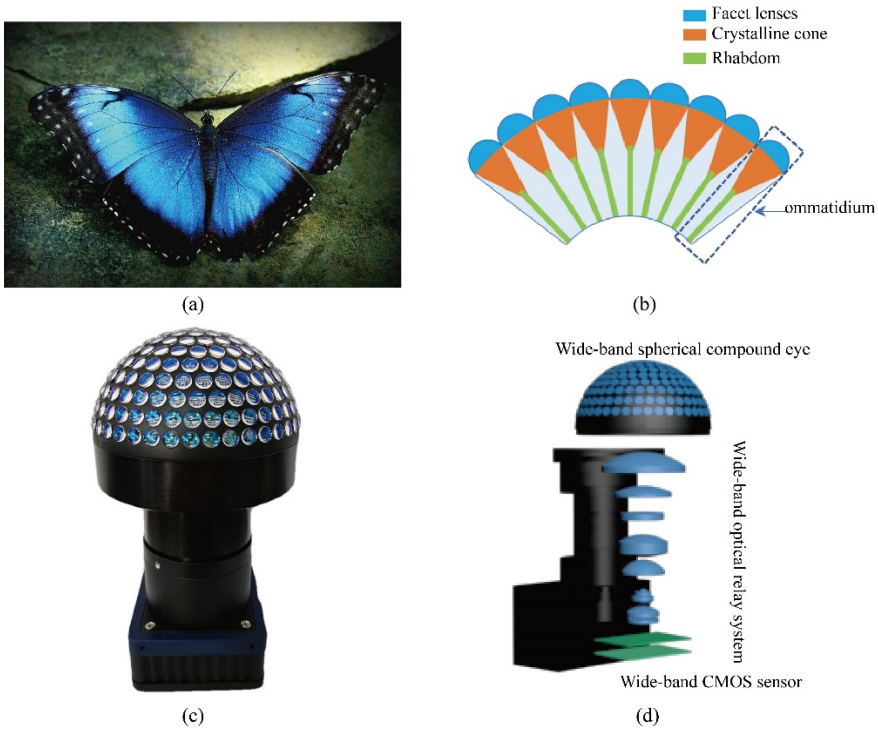

Fig. 1. (a) Morpho butterfly has a pair of compound eyes that can see a wide range of wavelengths covering ultraviolet, visible, and even NIR. (b) The butterfly's apposition compound eye is composed of numerous independent and non-interfering ommatidia, each of which consists of a facet lens, a crystalline cone, and a rhabdom with photoreceptor cells. (c) The picture of the fabricated prototype of the bio-inspired wide-band spherical compound eye camera. (d) Schematic diagram of the bio-inspired wide-band spherical compound eye camera.

2. Methods and materials

2.1. Optical design of the wide-band spherical compound eye camera

The wide-band spherical compound eye and the wide-band optical relay system are the main optical components of the wide-band spherical compound eye camera. The ray tracing of this optical design is shown in Fig. 2(a). The wide-band spherical compound eye collects light with wavelengths of 400nm-1000nm from a large field of view. Then the light was transformed onto an image sensor by the wide-band optical relay system. Optimized optical structure and appropriate materials can ensure the high-quality imaging of the camera in a wide range of wavelengths from visible light to NIR. The inherent merit of biological compound eyes, large field of view imaging, is inherited by this bionic camera.

In this optical design, ten sub-eyes were considered to simulate and calculate the optical performance of this wide-band spherical compound eye camera. The inter-ommatidia angle $\Delta\Phi$ is designed to be 8.57° and the acceptance angle $\Delta\varphi$ of each sub-eye is designed to be 16.74°. The total FOV of this wide-band spherical compound eye camera $FOV = \Delta\Phi \times 9 \times 2 + \Delta\varphi = 171°$ can be calculated. The theoretical effective cut-off frequency of this compound eye camera is given by formula (1).

$$N = \frac{1000}{2a}, \tag{1}$$

Optics EXPRESS

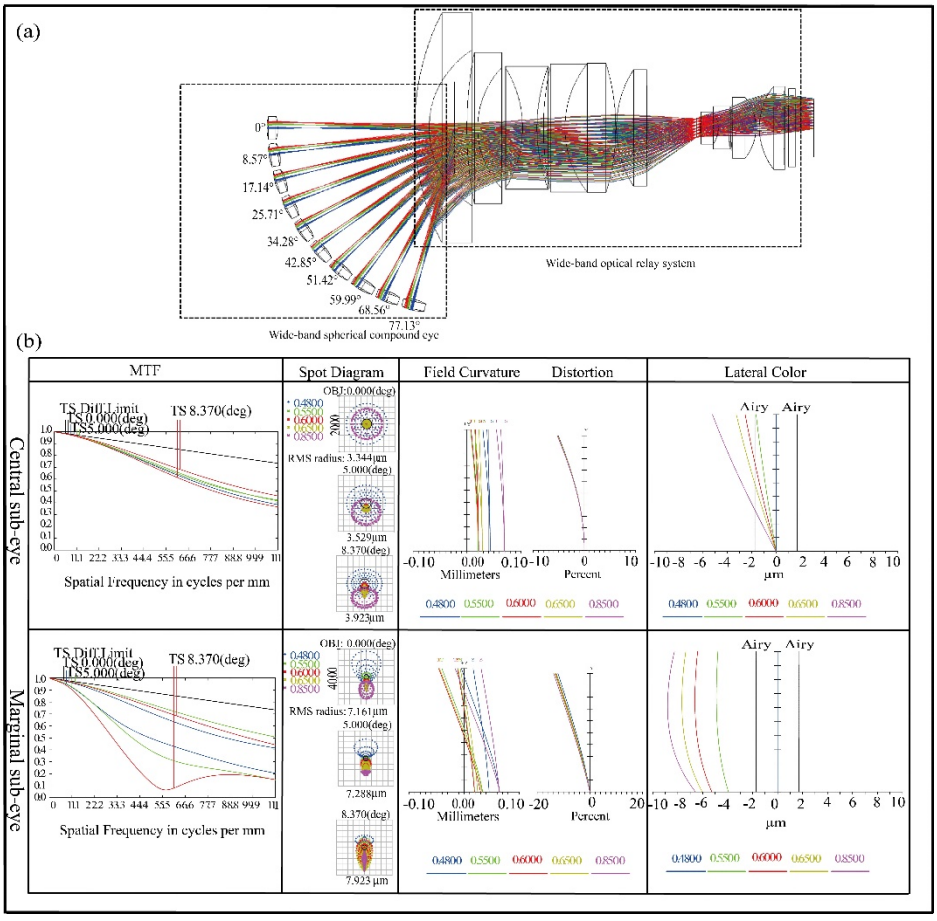

Fig. 2. (a) The optical ray tracing of the wide-band spherical compound eye camera. Ten sub-eyes were considered to simulate and calculate the optical performance of the optical system. The inter-ommatidia angle $\Delta\Phi$ is designed to be 8.57°. (b)The diagrams are MTF, spot diagrams, field curvature, and lateral color of the central sub-eye and the marginal sub-eye from left to right.

Optics EXPRESS

where N is the Nyquist cutoff frequency of this optical system, and a is the pixel size of the CMOS image sensor. The cutoff frequency of this compound eye camera is 111 lp/mm, when the pixel size of the image sensor is 4.5μm. The modulation transfer function (MTF), spot diagrams, field curvature, and lateral color are shown in Fig. 2(b) from left to right. The corresponding results of the central sub-eye and the marginal sub-eye are the top and bottom lines respectively. The MTF is studied to evaluate image quality. As can be seen, the MTFs are higher than 0.35 and 0.15 at the cutoff frequency for the central and marginal sub-eye respectively. The second column shows the Spot diagrams of the central and marginal sub-eye in different FOVs. As can be seen from the pictures, the root mean square (RMS) radii of these two sub-eyes are less than 3.923 μm and 7.923 μm, respectively. For each sub-eye, the focal spots are within a circular region with a diameter of 0.309 mm. It can be seen from the spot diagrams that there is a certain degree of separation between different wavelengths, indicating that the system has a certain chromatic aberration. To quantitatively analyze the chromatic aberration of the system, the lateral color was provided in Fig. 2(b). The rightmost column of Fig. 2(b) shows the lateral color curves of the center sub-eye and the margin sub-eye in maximum FOV. It can be seen that the value of the central sub-eye is less than 5.5 μm and the marginal sub-eye is less than 9 μm. These data show that the chromatic aberration of this system is controlled within a reasonable range and doesn't degrade image quality. The third column shows the field curvature and distortion in different FOVs for the central and marginal sub-eyes. It can be seen that the field curvature value of the central sub-eye is less than 0.0135mm, and the maximum distortion is less than 5.0991%. The field curvature of the marginal sub-eye is less than 0.0698 mm, and the maximum distortion value is less than 12.0981%. These results presented demonstrate that this optical design has a good imaging quality.

Tolerance analysis determines the difficulty of manufacturing and assembling accuracy of optical system, so tolerance analysis of the optical system is carried out based on ZEMAX software. The sensitivity model is employed to analyze the tolerance of the wide-band spherical compound eye camera. The diffraction MTF at 632.8nm is selected as the evaluation criterion for tolerance sensitivity analysis. The Monte Carlo method is used to perform a random simulation at a spatial frequency of 111 lp/mm. The results show that the thickness tolerance is ±20μm, the decenter and the tilt of lens element are ±10μm and ±0.1°, respectively. The tolerance is quite loose and common, so the manufacturing and assembling accuracy of the wide-band spherical compound eye camera can be easily guaranteed.

2.2. Prototype of the wide-band spherical compound eye camera

The Morpho butterfly's eye is an apposition compound eye which is made up of hundreds of ommatidia pointing along different directions, and each ommatidia is composed of a cornea, a crystalline cone, and a rhabdom with photoreceptor cells. A prototype of the wide-band spherical compound eye camera bio-inspired by the Morpho butterfly's eye is fabricated. This prototype, which can simultaneous capture visible and NIR images with a large field of view, is also composed of three parts: a wide-band spherical compound eye, a wide-band optical relay system, and a wide-band CMOS image sensor.

The wide-band spherical compound eye collecting light to form a compound eye image is the core of the prototype. The picture of the wide-band spherical compound eye is shown in Fig. 3(a). It contains 234 sub-eyes with a diameter of 6.35mm and a focal length of 10mm. These sub-eyes are made by traditional lens processing methods and were arranged in a circular arrangement on a 3D-printed resin spherical shell. Each sub-eye is formed by a wide band lens mounted in a stepped hole on a resin spherical shell. The wide band lens is made of L-BAL42 glass using traditional optical processing. Its transmission wavelength range is 400nm-1000 nm. The resin spherical shell with stepped holes is designed by SolidWorks and made by 3D printing. The stepped holes are arranged in a circle and face the center of the spherical shell. The interval between adjacent

Optics EXPRESS

stepped holes is determined by the inter-ommatidia angle. The resin spherical shell not only plays a role in supporting and fixing the sub-eye, but also prevents light crosstalk between adjacent sub-eyes. Figure 3(e) shows that the acceptance angle of each ommatidium is $\Delta\varphi$ =16.74 ° and the inter-ommatidia angle is $\Delta\Phi$ =8.57 °. There is overlapping field of view between adjacent sub-eyes, so one object can be captured by several sub-eyes. Therefore, this compound eye camera has the foundation and potential for target positioning and three-dimensional detection.

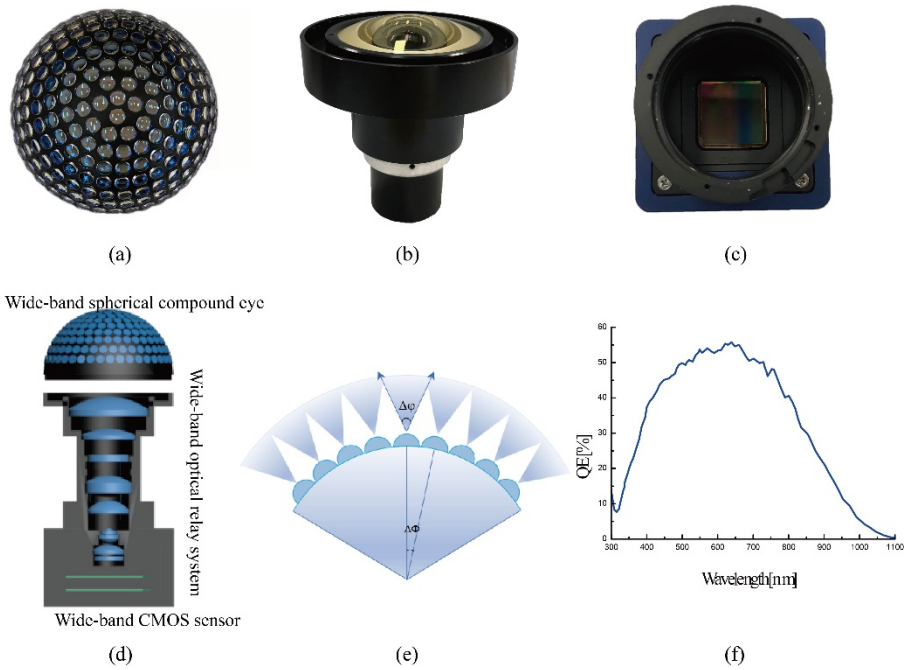

Fig. 3. The picture of (a) the wide-band spherical compound eye, (b) the optical relay system, and (c) the CMOS sensor. (d) The schematic diagram of the wide-band spherical compound eye camera. (e) FOV of each ommatidium and the inter-ommatidia angle. (f) The quantum efficiency of the CMOS sensor.

Imitating the crystalline cone, an optical relay system shown in Fig. 3(b) is introduced to re-image the curved compound eye image formed by the wide-band spherical compound eye on a CMOS sensor. The optical relay system is a telecentric optical system which consists of 9 groups of lenses. The focal length and total length of the optical relay system is 6.13 mm and 110mm respectively. It solves the problem of mismatch between the spherical compound eye and the planar CMOS sensor, and corrects aberrations of this camera.

An ON-Semiconductor Python NOIP1xx016KA CMOS image sensor (Resolution: 4096×4096, Pixel size:4.5μm, Frame rate:20fps) shown in Fig. 3(c) was adopted as the photoreceptor. This sensor is a near-infrared enhanced sensor which has high quantum efficiency in both visible and near-infrared bands. The quantum efficiency of this CMOS sensor shown in Fig. 3(f) reveals that it can respond to a wide wavelength range from 300 nm to 1000 nm covering ultraviolet, visible, and NIR. The working range of the entire system is jointly determined by the optical system and the sensor. The design and fabrication of the wide-band optical system is difficult, and the working wavelength of the optical system in the prototype is 400nm-1000 nm. However, the CMOS sensor has a wider working range covering 300nm-1000 nm. This makes the spherical compound eye camera have good scalability and provides a basis for further extend to the ultraviolet range. Moreover, a sensor with higher frame rate, such as ON-Semiconductor Python

Optics EXPRESS

NOIP1xx025KA (Frame rate:80fps, Pixel size: 4.5μm, Pixel resolution: 5120×5120, Wavelength range: 300nm-1000 nm), should be adopted for real-time imaging in practical applications. The sensor with lower frame rate is adopted in the prototype in the result of reducing costs without affecting the experimental results. Figure 3(d) shows the assembly diagram of this wide-band spherical compound eye camera. The fabricated prototype (see Fig. 1(c)) can realize visible and NIR imaging with a large field of view. The parameters of this prototype and other prominent prototypes are shown as Table 1.

Table 1. The parameters of our prototype and other prominent prototypes

Parameters	Our prototype	Ref. [24]	Ref. [7]	Ref. [12]
Number of ommatidia n	234	127	35	522
Pixels of each sub-image ν	100×100	135×135	214×214	80×80
Radius of the hemisphere R	50mm	68mm	-	2.5mm
Diameter of each ommatidium d	6.35mm	7.4mm	100μm	0.18mm
Focal length of each ommatidium f	10mm	-	170μm	-
Spatial resolution under VIS illumination	7lp/mm	-	-	-
Spatial resolution under NIR illumination	5lp/mm	-	-	-
Acceptance angle of each ommatidium $\Delta\varphi$	16.74°	14°	-	44°
The inter-ommatidia angle $\Delta\Phi$	8.57°	7°	-	-
FOV	**171°**	**98°**	**73°**	**170°**
Wavelength range λ	**0.4~1μm**	**0.42~0.7μm**	**0.4~0.7μm**	**0.4~0.7μm**
Size of the prototype S	7×7×18 cm^3	Φ12.3×17.3 cm^3	5.1×5×0.74mm^3	-
Pixel resolution	4096×4096	5120×5120	3280×2464	4912×3684

3. Results and discussion

The most distinguished feature of this prototype is that it is capable of simultaneous wide-band and large field of view imaging. The image outputted by this prototype is a compound eye image with 234 sub-images. In order to verify the optical performance of this prototype, a checkerboard pattern was used to measure the contrast of the compound eye image. Figure 4(a) and 4(b) show the compound eye images captured by the prototype under visible (400nm-700 nm) and NIR (850 nm) illumination, and the corresponding intensity profiles along the dotted lines for the center sub-images. The corresponding intensity profiles along the dotted lines clearly indicate that the visible image provide higher contrast than the NIR image. The Michelson contrast can be calculated by the formula (2).

$$Contrast = (I_{max} - I_{min})/(I_{max} + I_{min}), \tag{2}$$

where I_{max} is the maximum value of the intensity, I_{min} is the minimum value of the intensity. The calculated Michelson contrast is 0.91 for the visible image and 0.89 for the NIR image, respectively. Both visible image and NIR image have high contrast, although there are some differences. This declares that the prototype can clearly image under visible and NIR (850nm) illumination. To further verify the contrast of the margin sub-images under visible and NIR (850nm) illumination, Fig. 4(c) and 4(d) give the corresponding intensity profiles along the dotted lines for the margin sub-images. The calculated Michelson contrast of the margin sub-images is 0.86 for the visible image and 0.85 for the NIR image. There are small differences in the contrast of the visible and NIR images, as well as the contrast of the center and margin sub-images. The contrast difference between the center and margin sub-images is caused by the optical relay system.

Optics EXPRESS

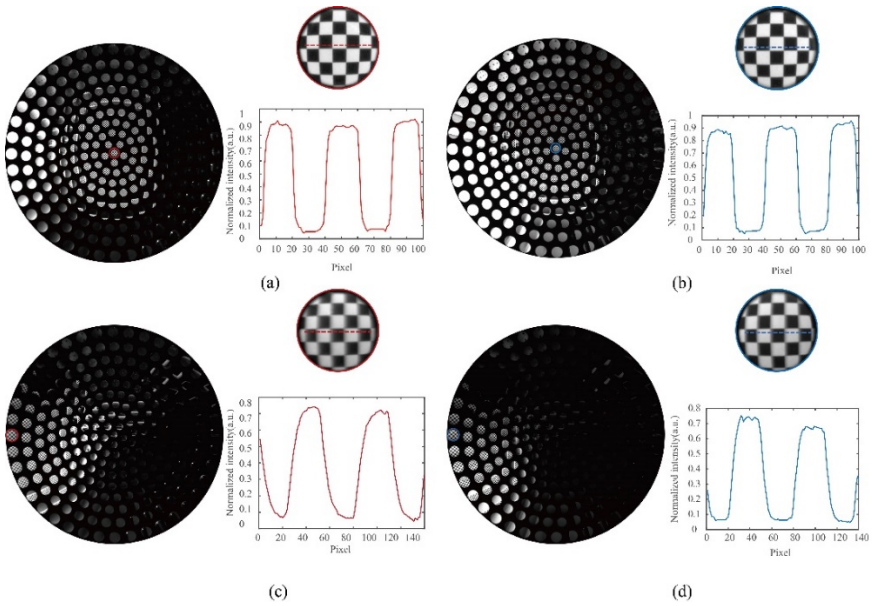

Fig. 4. The compound eye images captured by the prototype under visible (a) and NIR (b) illumination, and the corresponding intensity profiles along the dotted lines for the center sub-images. (c) and (d) are the corresponding intensity profiles along the dotted lines for the margin sub-images.

To further verify the image quality of this prototype, an ISO 12233 chart was used to measure the resolution of the camera. The ISO12233 chart is taken as the imaging target and placed about 8.5 cm away from the camera. The results show that the resolution of this prototype can reach 7lp/mm under visible illumination and 5lp/mm under NIR illumination (850 nm). The spatial resolution of the overall system is consistent with that of individual sub eye. There is slight aberration when the optical relay system converts the curved surface image formed by the compound eye array to the flat CMOS sensor. The contrast difference between visible and NIR images is caused by the difference in the transmittance of the optical system and the quantum efficiency of the CMOS sensor in these two wavelength ranges. The distortion of the central and margin sub-eye images is also slight, and the values of them are 5.34% and 8.2%, respectively. Traditional non-bio-inspired cameras with large field of view have severe distortion. The Canon fisheye lens (EF 8-15 mm f/4L USM) consists of 14 lenses in 11 groups, which is capable of 180° large field of view imaging. But its distortion value is as high as 50%. These quantization parameters indicate that this prototype has a good imaging performance without abnormal blurring and aberrations. Therefore, these results still clearly show that the margin sub-images still maintain high contrast and have a good image quality.

The 234 sub-images in the compound eye image are formed by 234 ommatidia pointing in different directions. This allows the prototype to shoot images with 171° field of view and makes it available for panoramic imaging. Figure 5(a) gives the schematic illustration of an experimental setup to demonstrate this key imaging characteristic. Three toys were placed at three different angular positions: -85.5° (left), 0° (center), and 85.5° (right). The corresponding compound eye image is shown in Fig. 5(b). The cup placed at the angular position of 0° is captured by the central ommatidium and other two toys are captured by the marginal ommatidia. The partial enlarged views in Fig. 5(b) show comparable clarity without anomalous blurring or aberrations. This kind of wide-field imaging without distortion is impossible to obtain using sophisticated fish-eye

Optics EXPRESS

lenses, spherical mirrors, or other specialized optics. Figure 5(c) is a laboratory picture taken randomly by this prototype. It also shows that the prototype's good definition in a wide-field angle.

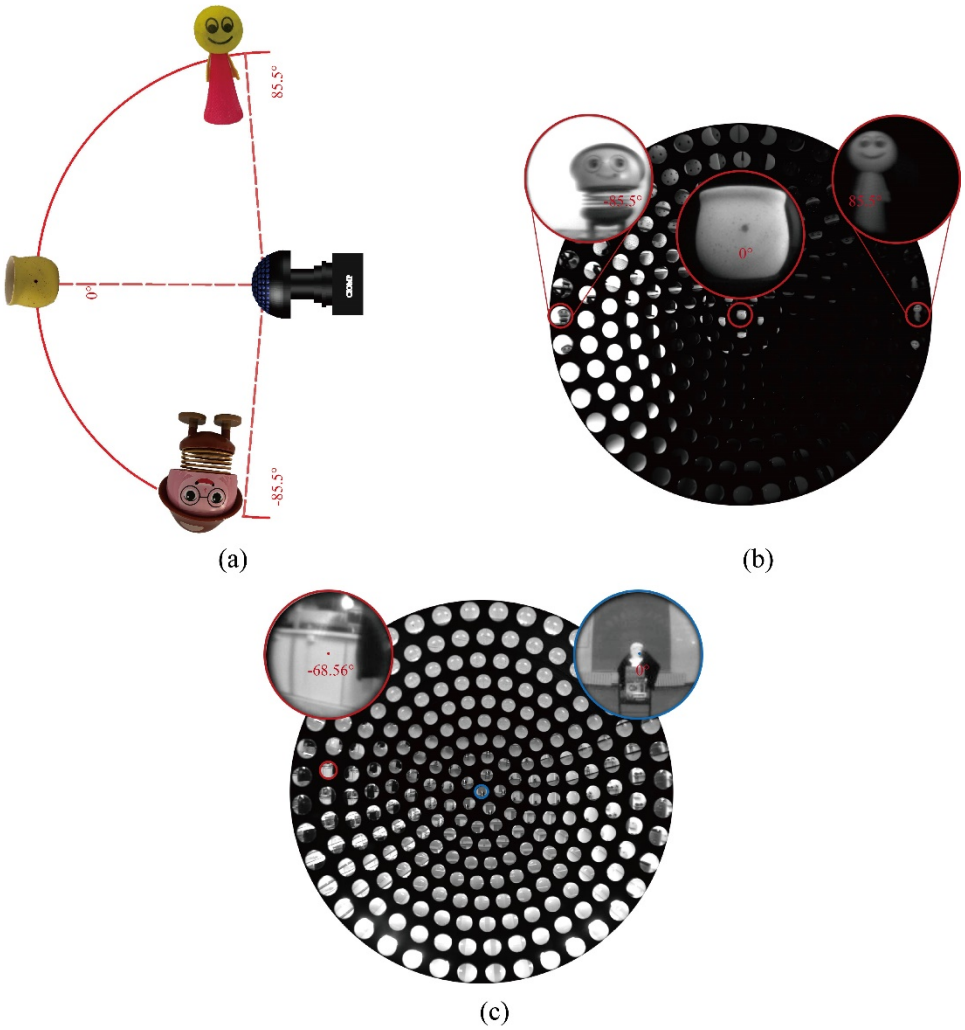

Fig. 5. (a) Schematic illustration of an experimental setup to demonstrate wide-field imaging characteristic. Three toys were placed at -85.5°, 0°, 85.8° respectively. (b) The corresponding compound eye image and partial enlarged views. (c) Laboratory picture taken by this prototype.

Another fascinating characteristic of this prototype is wide-band imaging with wavelengths range from visible to NIR. Extending to NIR makes the prototype have the potential for medical diagnosis. Figure 6(a) is the schematic illustration of an experimental setup to demonstrate vascular enhancement. A NIR light source (850nm) is used for auxiliary lighting. Figure 6(b) shows the compound eye image of human's arm and Fig. 6(d) is a partial enlarged view of this compound eye image. Figure 6(c) is the picture of human's arm photographed by a conventional camera. The experimental results clearly show that this prototype enables vascular enhancement imaging. In Fig. 6, vascular NIR imaging is to verify the wide band imaging performance of this compound eye camera. Wide-field and wide-band imaging technology is widely used in the

Optics EXPRESS

medical field, not only for near-infrared vascular imaging, but also for near-infrared fluorescence image guidance, large-field endoscopy, etc.

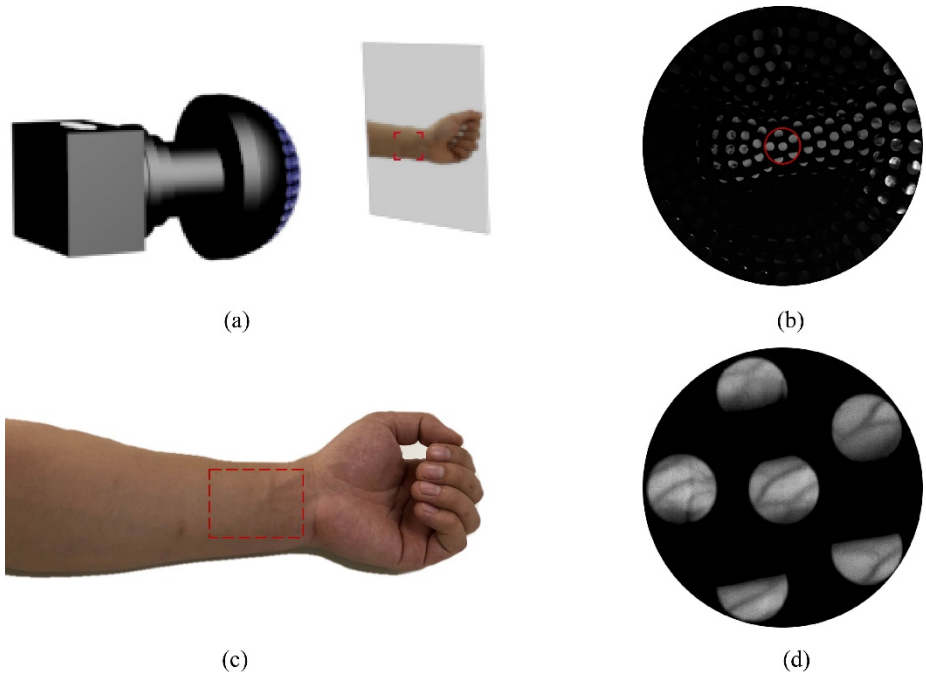

Fig. 6. (a) Schematic illustration of an experimental setup to demonstrate vascular enhancement. (b) The NIR compound eye image of human's arm captured by the prototype. (c) The picture of human's arm captured by a conventional smartphone. (d) Partial enlarged view of the NIR compound eye image.

4. Conclusion

A spherical compound eye camera inspired by the Morpho butterfly's apposition compound eyes is developed in this work. A prototype of this camera, which consists of three parts: a wide-band spherical compound eye with 234 sub-eyes for light collection, a wide-band optical relay system for light transmission, and a wide-band CMOS image sensor for photoelectric conversion, is fabricated. This prototype is capable of achieving a large field of view ($360° \times 171°$) imaging over a wide range of wavelengths from 400nm to 1000nm. The results presented show that this prototype enables large field of view imaging without anomalous blurring or aberrations, and vascular enhancement imaging. Due to the excellent characteristics of wide-band and wide-field of view imaging, this spherical compound eye camera has huge potential in the fields of target detection, recognition, surveillance, reconnaissance, and medical diagnosis. The architecture proposed in this prototype is capable of wide band and large field of view imaging without anomalous blurring or aberrations, but also exists some fundamental limits such as complex structure and waste of some pixels. The system errors caused by the employment of the relay optical system is difficult to eliminate. This results in a slight blur and distortion still present in the system. Research on compound eye image processing can alleviate the impact of these errors. The focus of our next work is restoring the panoramic image, extending the camera to the ultraviolet band, and developing a wide-band multi-spectral camera. Other important direction for future research is developing bioinspired sensors to better match compound eye optics array and improve the performance of the compound eye cameras.

Optics EXPRESS

Funding. National Natural Science Foundation of China (62005277); CIOMP-Fudan University Joint Fund (Y9R733N190).

Disclosures. The authors declare no conflicts of interest.

Data availability. Data underlying the results presented in this paper are not publicly available at this time but may be obtained from the authors upon reasonable request.

References

1. Y. Cheng, J. Cao, Y. K. Zhang, and Q. Hao, "Review of state-of-the-art artificial compound eye imaging systems," Bioinspir. Biomim. **14**(3), 031002 (2019).
2. Q. Yang, M. Li, H. Bian, J. Yong, F. Zhang, X. Hou, and F. Chen, "Bioinspired Artificial Compound Eyes: Characteristic, Fabrication, and Application," Adv. Mater. Technol. **6**(10), 2100091 (2021).
3. L. P. Lee and R. Szema, "Inspirations from biological optics for advanced photonic systems," Science **310**(5751), 1148–1150 (2005).
4. K. H. Jeong, J. Kim, and L. P. Lee, "Biologically inspired artificial compound eyes," Science **312**(5773), 557–561 (2006).
5. A. Borst and J. Plett, "OPTICAL DEVICES Seeing the world through an insect's eyes," Nature **497**(7447), 47–48 (2013).
6. R. Horisaki, S. Irie, Y. Ogura, and J. Tanida, "Three-dimensional information acquisition using a compound imaging system," Opt. Rev. **14**(5), 347–350 (2007).
7. K. Kim, K. W. Jang, J. K. Ryu, and K. H. Jeong, "Biologically inspired ultrathin arrayed camera for high-contrast and high-resolution imaging," Light: Sci. Appl. **9**(1), 28 (2020).
8. K. Kim, K.-W. Jang, S.-I. Bae, H.-K. Kim, Y. Cha, J.-K. Ryu, Y.-J. Jo, and K.-H. Jeong, "Ultrathin arrayed camera for high-contrast near-infrared imaging," Opt. Express **29**(2), 1333 (2021).
9. J. Tanida, R. Shogenji, Y. Kitamura, K. Yamada, M. Miyamoto, and S. Miyatake, "Color imaging with an integrated compound imaging system," Opt. Express **11**(18), 2109–2117 (2003).
10. L. C. Kogos, Y. Li, J. Liu, Y. Li, L. Tian, and R. Paiella, "Plasmonic ommatidia for lensless compound-eye vision," Nat. Commun. **11**(1), 1637 (2020).
11. Y. M. Song, Y. Xie, V. Malyarchuk, J. Xiao, I. Jung, K. J. Choi, Z. Liu, H. Park, C. Lu, R. H. Kim, R. Li, K. B. Crozier, Y. Huang, and J. A. Rogers, "Digital cameras with designs inspired by the arthropod eye," Nature **497**(7447), 95–99 (2013).
12. B. Dai, L. Zhang, C. Zhao, H. Bachman, R. Becker, J. Mai, Z. Jiao, W. Li, L. Zheng, X. Wan, T. J. Huang, S. Zhuang, and D. Zhang, "Biomimetic apposition compound eye fabricated using microfluidic-assisted 3D printing," Nat. Commun. **12**(1), 6458 (2021).
13. Y. Zhang, H. Xu, Q. Guo, D. Wu, and W. Yu, "Biomimetic multispectral curved compound eye camera for real-time multispectral imaging in an ultra-large field of view," Opt. Express **29**(21), 33346–33356 (2021).
14. X. Yu, C. Liu, Y. Zhang, H. Xu, Y. Wang, and W. Yu, "Multispectral curved compound eye camera," Opt. Express **28**(7), 9216–9231 (2020).
15. H. Deng, X. Gao, M. Ma, Y. Li, H. Li, J. Zhang, and X. Zhong, "Catadioptric planar compound eye with large field of view," Opt. Express **26**(10), 12455–12468 (2018).
16. C.-C. Huang, X. Wu, H. Liu, B. Aldalali, J. A. Rogers, and H. Jiang, "Large-Field-of-View Wide-Spectrum Artificial Reflecting Superposition Compound Eyes," Small **10**(15), 3050–3057 (2014).
17. M. Giurfa, G. Zaccardi, and M. Vorobyev, "How bees detect coloured targets using different regions of their compound eyes," J. Comp. Physiol., A **185**(6), 591–600 (1999).
18. A. Kapustjansky, L. Chittka, and J. Spaethe, "Bees use three-dimensional information to improve target detection," Naturwissenschaften (1913-2014) **97**(2), 229–233 (2010).
19. M. Garcia, C. Edmiston, T. York, R. Marinov, S. Mondal, N. Zhu, G. P. Sudlow, W. J. Akers, J. Margenthaler, S. Achilefu, R. G. Liang, M. A. Zayed, M. Y. Pepino, and V. Gruev, "Bio-inspired imager improves sensitivity in near-infrared fluorescence image-guided surgery," Optica **5**(4), 413–422 (2018).
20. M. S. Kim, M. S. Kim, G. J. Lee, S.-H. Sunwoo, S. Chang, Y. M. Song, and D.-H. Kim, "Bio-Inspired Artificial Vision and Neuromorphic Image Processing Devices," Adv. Mater. Technol. **7**(2), 2100144 (2022).
21. H. H. Thoen, M. J. How, T. H. Chiou, and J. Marshall, "A Different Form of Color Vision in Mantis Shrimp," Science **343**(6169), 411–413 (2014).
22. I. M. Daly, M. J. How, J. C. Partridge, S. E. Temple, N. J. Marshall, T. W. Cronin, and N. W. Roberts, "Dynamic polarization vision in mantis shrimps," Nat. Commun. **7**(1), 12140 (2016).
23. M. Garcia, C. Edmiston, R. Marinov, A. Vail, and V. Gruev, "Bio-inspired color-polarization imager for real-time in situ imaging," Optica **4**(10), 1263–1271 (2017).
24. H. Xu, Y. Zhang, D. Wu, G. Zhang, Z. Wang, X. Feng, B. Hu, and W. Yu, "Biomimetic curved compound-eye camera with a high resolution for the detection of distant moving objects," Opt. Lett. **45**(24), 6863–6866 (2020).